Toxicity of Zirconia oxide Nanoparticles: Liver Biodistribution and Liver Damages

Ting Sun
Nanfang Hospital, southern medical university https://orcid.org/0000-0003-1668-7751
Lingling Ou
the first affiliated hospital, jinan university
Xiaozhen Zhan
Southern Medical University Nanfang Hospital
Wenxin Zhao
the first affiliated hospital, JINAN university
Rui Huang
the first affiliated hospital, jinan university
Xiaoli Feng
Stomatological hospital, SHOUTHERN MEDICAL UNIVERSITY
Jia Liu
STOMATOLOGICAL HOSPITAL, SOUTHERN MEDICAL UNIVERSITY
Suhan Yin
STOMATOLOGICAL HOSPITAL, SOUTHERN MEDICAL UNIVERSITY
Xiangning Liu
the first affiliated hospital, jinan university
Renfa Lai
the first affiliated hospital, jinan university
Longquan Shao (shaolongquan@smu.edu.cn)
Stomatological Hospital, Southern Medical University, Guangzhou 510280, China

Research

Keywords: Zirconia, Nanoparticle, Liver, Biodistribution, Toxicity

Posted Date: January 29th, 2020

DOI: https://doi.org/10.21203/rs.2.22142/v1

Abstract

Background: Zirconia nanoparticles (ZrO_2-NPs) have been increasingly used in industrial, biomedical and dental materials. However, the scientific basis for the toxicological effects of ZrO_2-NPs is poorly elucidated, and the understanding of the underlying mechanism is still limited.

Results: The hepatic biodistribution and toxicological effects of ZrO_2-NPs after intravenous administration (20mg/kg bw) in vivo and the toxicological mechanism toward hepatocytes in vitro were investigated. The liver showed continuous ZrO_2-NP accumulations liver over a 28-d period. Moreover, ZrO_2-NPs induced oxidative stress and increased inflammatory responses and functional injury in the liver. Hepasteatosis and cell death were observed in histopathological and immunohistochemical studies. RNA-seq identified the main pathways involved in the metabolism, cellular process, and human diseases. The RT-qPCR analysis results showed that ZrO_2-NP exposure caused the upregulation of P53, Foxo1, Gadd45g, P21, Caspase3, and PPARα and the downregulation of Igfbp2 and Akt in the liver in response to the ZrO_2-NP treatment. Meanwhile, the results of the in vitro studies demonstrated that ZrO_2-NPs exposure resulted in cytotoxicity in Hepg2 cells in a dose- and time-dependent manner. ZrO_2-NPs were proven to induce oxidative stress, lipid accumulation, cell cycle arrest and cell apoptosis to Hepg2 cells. Western-blot analysis further proved the depression of Igfbp2, activation of Akt-mediated signaling pathway and P53-mediated signaling pathway for Hepg2 cells exposure to ZrO_2-NPs.

Conclusions: This study proves that ZrO_2-NPs have negative impacts on the liver and exhibit potential risks for non-alcoholic fatty liver disease (NAFLD). There is potential concern over ZrO_2-NPs' hepatoxicity in biomedical applications and occupational exposure through large-scale production.

Background

ZrO_2 nanoparticles (ZrO_2-NPs) have resulted in outstanding developments in the fields of industrial, biomedical and dental applications in recent years. Industrial uses of ZrO_2-NPs include applications in foundry sands, refractories, and ceramics. ZrO_2-NPs are also applied in biomedicine and dentistry, e.g., in the coatings of hip joint endoprostheses, dental prostheses, bone defect materials, biosensors and drug-loaded carriers [1-4]. However, NPs are difficult to degrade and can easily accumulate in organs. Because of their huge surface areas, NPs impact enzymes and other proteins, disrupting a series of biological processes in the body [5, 6]. Thus, the extensive use of ZrO_2-NPs may lead to environmental and human exposure, raising concerns about their potential impact and toxicity, especially via occupational exposure during manufacturing.

Studies have proven the potential toxicity of ZrO_2-NPs. Alzahrani et al. [7] reported the apoptotic and DNA-damaging effects of yttria-stabilized ZrO_2-NPs on human skin epithelial cells. Ye et al. [8] showed that ZrO_2-NPs could induced ROS productions and apoptosis effects, which may have an impact on osteogenesis in Osteoblast-Like 3T3-E1 Cells. Yang et al. [9] reported that hollowed ZrO_2-NPs induced

oxidative damage in mice after intravenous injection. However, the scientific basis for the toxicological effects of ZrO_2-NPs is poorly elucidated, and the understanding of the underlying mechanism is still finite, posing far-reaching challenges to their practical application. Our previous study investigated the distribution of ZrO_2-NPs in various organs (including the spleen, heart, brain, kidney and lung) and proved that ZrO_2-NPs exposure could induce oxidative stress, cell death and gene expression changes in various organs [10].

The liver provides the critical function of catabolism and biliary excretion of blood-borne particles, as well as serves as an important site for the elimination of foreign substances and particles [11]. Thus, the liver is a primary target organ in NPs distribution [12, 13]. NPs can reach the liver through blood circulation or translocation from the other organs [13-15]. Therefore, full research on the hepatotoxicity of ZrO_2-NPs and, especially, the potential molecular mechanisms is needed. Meanwhile, the biodistribution and clearance of ZrO_2-NPs in the liver has not been clearly illustrated. The general scheme of NPs uptake and clearance occurs through three main mechanisms: renal, hepatobiliary, and mononuclear phagocyte system (MPS) mechanisms [14, 16]. NPs can traverse the hepatic sinusoid and are primarily taken up by MPS after administration into the body. Depending on their physicochemical properties, NPs may filter out into the space of Disse and be endocytosed by hepatocytes. NPs are eventually eliminated through hepatobiliary or renal clearance [17]. As inorganic NPs, ZrO_2-NPs have more stable cores and thus are almost non-degradable. Therefore, ZrO_2-NPs are more likely to be retained in the liver for a long term.

In the present study, the distributions of ZrO_2-NPs in rat livers after intravenous administration and the consequent potential particle-induced injuries and function alterations were estimated. RNA-Seq analysis and precious gene expression analysis of the liver were also conducted. Based on the outcomes of the in vivo studies, in vitro studies were further conducted using ZrO_2-NPs incubated with Hepg2 cells to explore the mechanisms of ZrO_2-NPs-induced liver damage. Therefore, this study provides overall insight into the hepatic effects of ZrO_2-NPs.

Materials And Methods

Characterization of ZrO_2-NPs. ZrO_2-NPs were purchased from Sigma-Aldrich Chemical Company (Saint Louis, MO, USA) at 100.0% purity. The detailed characterization of the physicochemical properties of the ZrO_2-NPs was reported in our previous study [10].

In Vivo Studies

Animal and Intravenous Injections. Seventy adult male Wistar rats (w 200.0±20 g each) were purchased from the Laboratory Animal Center, Southern Medical University, Guangzhou, China. All procedures involving animals were approved by the Institutional Animal Care and Use Committee of Jinan University. The ZrO_2-NPs were primarily sterilized by gamma-ray radiation. Thereafter, the injection suspensions were prepared through the dispersion of ZrO_2-NPs in 0.5% normal saline (NS). A single tail-vein injection

of ZrO_2-NPs (20 mg/kg-bw) was slowly administered to the rats. The rats were randomly divided into seven groups (ten in each group), including one control group. A group of ten animals injected with 0.5% NS was used as the controls. The rats were then sacrificed at six time points after the intravenous injections.

Perfusion and Harvesting of Tissues. The rats were deeply anesthetized by intraperitoneal injection of 2.3 mL of 6 mg/mL Nembutal. The rats were then sacrificed at six time points, i.e., 1 d, 3 d, 7 d, 10 d, 14 d and 28 d, after ZrO_2-NP injection. Approximately 2-3 mL of blood was collected through cardiac puncture, and the rats were perfused through the left cardiac ventricle with NS until the venous return was clear. The liver tissues were harvested. All instruments and samples were thoroughly washed with water during harvesting to minimize adherent ZrO_2-NPs. The samples were placed in cleaned Eppendorf tubes. The tubes were snap-frozen in liquid nitrogen and stored at -80°C until analysis.

Quantification of ZrO_2-NPs in the Liver. The liver samples were weighed and then subjected to microwave-assisted digestion and inductively coupled plasma mass spectrometry (ICP-MS) analysis. Briefly, the collected tissues (200 mg per sample) were primarily pre-digested overnight in concentrated nitric acid and H_2O_2 in an oven chamber. After digestion, the mixed solutions were then heated at 160°C using a high-pressure reaction container until the samples were completely digested. The solutions were then heated at 120°C until the remaining nitric acid was nearly evaporated to dryness. The resulting solutions were finally diluted to 2 mL with 1% nitric acid + 0.1% Triton-100 and analyzed using ICP-MS. Calibration standards of six Zr concentrations (0.05, 0.1, 0.2, 0.4, 0.6 and 0.8 mg/L) were analyzed with each batch of samples. Each sample was spiked with 0.2 mg/L Ge as an internal standard.

Measurement of Cytokines. TNF-α, IL-1α, IL-1β, IL-6 and IL-8 in the liver after treatment with ZrO_2-NPs and physiological saline for different intervals were measured using an enzyme-linked immunosorbent assay (ELISA) kit specifically for rats (Jiancheng Bioengineering Institute, Nanjing, China). The assays were performed following the manufacturer's instructions.

Ultrastructure Observation. Liver samples were fixed in 3% glutaraldehyde + 2% paraformaldehyde for 2 h. Small pieces of tissue (approximately 1 mm^3) collected from these samples were washed with 0.1 mol/dm^3 cacodylate buffer (pH 7.2-7.4) and post fixed in 1% osmium tetraoxide for 1 h. The samples were then dehydrated using a series of ethanol concentrations and embedded in Epon resin. Finally, TEM (H-7500, Hitachi, Tokyo, Japan) was used to visualize the ultrathin sections.

Histopathology and Immunohistochemical Analysis. The histological specimens were prepared as follows. Formalin-fixed samples were dehydrated with gradient solutions of ethanol and then embedded in paraffin. The tissue specimens were sliced with an automatic microtome and then stained with hematoxylin and eosin (H&E) for conventional morphological evaluation. Representative photos were captured with a charge-coupled device (CCD) digital camera fixed to a light-microscopy system (IX73, Olympus, Tokyo, Japan).

Furthermore, immunohistochemistry analysis was carried out to identify the specific toxicity effects. Proliferating cell death in tissues was determined using a Ki-67 assay kit (Abcam, Cambridge, MA, USA) according to the manufacturer's instructions. Tissue sections were primarily incubated with the Ki-67 monoclonal antibody. Proliferating cells were stained with the Ki-67 monoclonal antibody. The mean positive-staining density was analyzed in randomly selected areas in each section at ×400 magnification using image analysis software (Image Pro Plus 7.0; Media Cybernetics, Rockville, MD, USA). The ratios of positively stained cells were determined according to the positively stained cell numbers divided by the total cell numbers.

Apoptotic cell death in tissues was determined using the Tunel assay kit (Promega, Madison, WI, USA) according to the manufacturer's instructions. After incubation in the Tunel solution, tissue sections were immersed in 0.3% hydrogen peroxide in PBS and then incubated with peroxidase solution for 30 min at room temperature. Tissue sections were stained with 0.1% DAB solution and counterstained with hematoxylin. The presence of apoptotic cells was calculated. Positive-staining (brown) photographs were captured in randomly selected fields with image analysis software (Image Pro Plus 7.0, Media Cybernetics, Rockville, MD, USA).

Liver function assay. The levels of alanineaminotransferase (ALT), aspartate-aminotransferase (AST) and (lactate dehydrogenase, LDH) in serum were determined using a chemistry-immuno analyzer (VITROS 5,1 FS, Ortho-Clinical Diagnostics, NY, USA).

RNA-Seq Quantification. RNA-Seq quantifications of the expressed genes of the live samples were conducted 7 d post injection. Three samples of livers from rats injected with a single dose of ZrO_2-NPs were harvested 7 d post injection. The samples were individually matched to tissues from noninjected control animals of a similar weight. The total RNA was isolated using TRIzol reagent (Invitrogen, CA, USA) according to the manufacturers' instructions. RNA was stored at -80°C. The RNA was then submitted to the BGI Genomics Core Facility Lab. mRNA with a polyA tail was primarily selected to remove the DNA probe. After purification, the targeted RNA was fragmented and then reverse transcribed into double-stranded cDNA (dscDNA) using an N6 random primer (BGI Genomics, Shenzhen, China). The dscDNA was end-repaired with phosphate at the 5' end and sticky 'A's at the 3' end. The PCR product was denatured by heat. The single-stranded DNA was then cyclized by splint oligo and DNA ligase. The RNA quality was analyzed using an Agilent 2100 Bioanalyzer (Agilent, Beijing, China). Sequencing qualification was then performed with the Gene Sequence Detector System BGI-SEQ 500 (BGI Genomics, Shenzhen, China). Differentially expressed genes (DEGs) were screened through the NOISeq method [18], with the default criteria for DEGs as follows: fold change ³2 and divergence probability ³0.8. Gene ontology (GO) and pathway enrichment analyses of the DEGs were performed using the PANTHER classification system (http://www.pantherdb.org/data/) and Kyoto Encyclopedia of Genes and Genomes (KEGG) (http://www.kegg.jp/).

RT-qPCR Analysis. Based on the RNA-Seq quantification results, precise quantification of the gene expressions in the liver tissue was then conducted. The liver samples were kept at -80°C until analysis.

Frozen tissues were homogenized and extracted using TRIzol Reagent (Gibco, Waltham, MA, USA) according to the manufacturer's instructions. The extracted RNA was further purified using the Qiagen TM RNeasy Mini Kit (Dusseldorf, Germany) to remove any genomic DNA contamination. The total RNA was measured at 260 and 280 nm using an M5 spectrophotometer (Molecular Devices, Sunnyvale, CA, USA). The purity of the RNA sample was measured according to the 260/280 nm ratio, with expected values between 1.8 and 2.0. Synthesized complementary DNA (cDNA) was prepared from RNA samples (1000 ng) using the Prime Script TM RT Reagent Kit (TaKaRa, Tokyo, Japan). RT-qPCR was carried out using a commercial kit (SYBR Premix Ex Taq II, TaKaRa, Tokyo, Japan) and analyzed on a Lightcycler 480 Sequence Detector System (Roche, Basel, Switzerland). The amplification protocol was performed as follows: after 30 s of incubation at 94°C to activate the Hot Start DNA polymerase, 40 cycles of amplification were accomplished over 5 s at 94°C for denaturation and over 30 s at 60°C for annealing (fluorescence detection). The expression level of each target gene was normalized to its β-actin mRNA content. The primers used for PT-PCR are shown in Tab. 1.

In Vitro Studies

Cell Culture Treatment with ZrO_2-NPs. The Hepg2 cell line (HB-8065) was obtained from the American type culture collection (ATCC). Hepg2 cells were cultured in Dulbecco's Modified Eagle Medium (DMEM) containing 10% fetal bovine serum, 1% penicillin/streptomycin, 1% L-glutamine, and 1% non-essential amino acids in a humidified atmosphere of 5% CO_2 at 37°C. The media was changed every 3 days. Cells were removed from the culture dishes by rinsing in PBS and incubating in trypsin-EDTA solution. Cells were seeded onto each test substrate at 1×10^5 cells/ml in the same media for all assays. The ZrO_2-NPs were sterilized by gamma-ray radiation and suspended in the culture medium. The stock solutions were then serially diluted to yield doses of 250 μg/ml. These samples were sonicated before exposure to the cells. After the cells were attached for 24 h in the full medium, the freshly dispersed ZrO_2-NP suspensions were immediately applied to the cells. Cells free of ZrO_2-NPs were set as the control.

Lipid Analysis. The total cholesterol (TC) and triglyceride (TG) levels in the supernatants of the HepG2 cells were determined by ELISA (Jiancheng Bioengineering Institute, Nanjing, China).

Intracellular ROS Measurement and Oxidative Stress. The reactive oxygen species (ROS) levels of the untreated control and ZrO_2-NP-treated cells were determined by chemiluminescence using the Reactive Oxygen Species Assay Kit (Jiancheng Bioengineering Institute, Nanjing, China) after 6 h of exposure. The SOD and MDA levels were independently measured using the reagent kits (Jiancheng Bioengineering Institute, Nanjing, China) after 24 h of exposure.

Cell-Cycle and Apoptosis Analyses. After incubation for 24 h, the cells were harvested by trypsinization and fixed with 70% ice-cold ethanol for 10 min at 4°C. After washing, the cell pellets were resuspended in propidium iodide (PI) staining buffer and incubated for 15 min at 37°C. The cell-cycle distributions were analyzed by a fluorescence-activated cell sorter (FACS; Gallios, Beckman Coulter, Brea, CA, USA) and Multicycle Mod Fit software (Beckman Coulter, Brea, CA, USA). The untreated control and ZrO_2-NP-

exposed cells were treated with cisplatin (20 mg/mL) for 24 h and then washed and resuspended. Then, 5 μL of annexin V-FITC conjugate and 10 μL of PI solution were added to 500 μL of each cell suspension, followed by incubation at room temperature for 15 min in the dark. Flow cytometry analysis was performed with FACS and analyzed by FlowJo express software (FlowJo LLC, Ashland, Oregon, USA).

Western-Blot Analysis. The Hepg2 cells were lysed in ice-cold protein lysis buffer (P0013, Biyuntian, Shanghai, China). After centrifuging the lysates at 12,000 rpm at 4°C for 10 min, the supernatants were collected and stored at -80°C until use. The lysates were then transferred to PVDF membranes. The membranes were incubated with 5% milk in PBS for 1 h and then incubated with primary antibodies overnight at 4°C. The following primary antibodies were used: anti-P53 (2524S, CST, Danvers, MA, USA), anti-P21 (ABS135943a, Absin, Shanghai, China), anti-Gadd45g (ABS132755a, Absin, Shanghai, China), anti-Bcl6 (sc-7388, Santa Cruz, Santa Cruz, CA, USA), anti-Foxo1 (2880S, Cell Signaling, Danvers, MA, USA), anti-Bcl2 (SC7382, Santa Cruz, Santa Cruz, CA, USA), anti-Bax (sc- 20067, Santa Cruz Biotechnology, Santa Cruz, CA, USA), Caspase 3 (sc-7272, Santa Cruz Biotechnology, Santa Cruz, CA, USA), anti-Akt (ab8805; Abcam, France), anti-Irs2 (sc-390761, Santa Cruz Biotechnology, Santa Cruz, CA, USA), anti-Igfbp2 (sc-25285, Santa Cruz Biotechnology, Santa Cruz, CA, USA) and anti-Gapdh (AB8245, Abcam, Cambridge, MA, USA). Blots were incubated with peroxidase-coupled secondary antibodies (BA1054, Boster, Pleasanton, CA, USA) for 1 h, and the protein concentration was measured using a bicinchoninic acid protein assay kit (23227, Thermo, Rockford, IL, USA).

Statistical Analysis. The data were analyzed using one-way ANOVA with Turkey's HSD multiple comparison post-hoc tests, with $P < 0.05$ or $P < 0.01$ considered significant (SPSS v. 22.0, SPSS, Chicago, IL, USA).

Results

Characterization of ZrO_2-NPs. The TEM micrographs of ZrO_2-NPs are shown in Fig. 1. The ZrO_2-NPs were spherical with an average diameter of approximately 38 nm [10]. More detailed physicochemical properties of the ZrO_2-NPs were reported in our previous study [10].

Dose of ZrO_2-NPs adopted in this study. To date, very few data about the dose of ZrO_2- NPs administration is available. In a recent study, mice were intravenously injected with hollowed ZrO_2-NPs at single doses (100-500 mg/kg-bw) [9]. In the liver, it was reported that a single dose of NPs showed lower single-dose toxicity compared to that from multiple doses of NPs administration [19]. A dose of 20 mg/kg-bw ZrO_2- NPs was chosen, since this was the dose used in our previous study without eliciting abnormal behavior from the rats [10]. Thus, the single dose of 20 mg/kg-bw ZrO_2- NPs adopted in this study is a relative low dose. A dose of 20 mg/kg-bw in rats is equivalent to a human dose of 0.32 mg/kg bw, corresponding to approximately 19 mg for a human of 60 kg, according to the guidelines for dose translation from animals to humans.

Biodistribution of ZrO_2-NPs. Fig. 2A demonstrates the biodistributions of the ZrO_2-NPs accumulated in the liver at six time points after a single injection of ZrO_2-NPs. The liver captured high amounts of ZrO_2-NPs during a 28-d period post administration. Reportedly, the liver acts as a biological filtration system that sequesters 30-99% of administered nanoparticles from the bloodstream [13]. As inorganic NPs, ZrO_2-NPs have more stable cores and are thus almost non-degradable. Therefore, in the present study, ZrO_2-NPs persisted in the liver for at least a 28-d retention. Reportedly, inorganic NPs, such as gold [20] and iron oxide-coated NPs [21] could remain in the liver for 2-6 months after administration. From 1d to 10 d after administration, the contents in the liver gradually increased, reached a peak at 10 d, and then decreased (Fig. 2A). Meanwhile, our previous study proved that the ZrO_2-NPs accumulation in the lung began to decrease from 10 d after exposure [10]. The lungs primarily maintained high levels of ZrO_2-NPs due to the lipophilic property of lung-lining fluid [22]. After acute exposure, the NPs can be translocated out of the lungs through lymphatic vessels [23] and/or the bloodstream to other organs over time. This can explain why the levels of ZrO_2-NPs in the liver gradually increased and reached a peak at 10 d. Additionally, the levels of ZrO_2-NPs in the liver began to decrease after 10 d post injection, which could have resulted from the elimination of ZrO_2-NPs from the body.

NPs (<6 nm) can be cleared from the kidneys by renal clearance [24]. The MPS has been proven to take up NPs of a broad size scale spanning several hundreds of nanometers [25, 26]. NPs smaller than the diameter of liver sinusoidal fenestrations (up to 150-200 nm) can extravasate into the space of Disse and interact directly with hepatocytes [27]. Thus, in the present study ZrO_2-NPs (with a diameter of 38 nm) are more likely to be taken up and retained by the MPS or hepatocytes. If NPs are degradable by the MPS, their substituents may escape sequestration and return to blood circulation for eventual hepatobiliary or renal clearance. In hepatobiliary clearance, hepatocytes breakdown NPs and excrete them into the bile via the biliary system, after which the NPs traverse the entire gastrointestinal tract and are eliminated in feces [28]. Our previous study proved that feces showed ZrO_2-NPs accumulations during a 28-d period post administration. However, no ZrO_2-NPs accumulation was detected in the kidneys or urine [10]. Based on these results, we believe ZrO_2-NPs were cleared by hepatobiliary route in the present study.

Oxidative Damage and Inflammatory Responses in the Rat Liver. The time-course profiles of the SOD activities and MDA levels in the liver at six time points after a single injection of ZrO_2-NPs were evaluated (Fig. 2B, C). Fig. 2B, C shows that oxidative stress responses were detected at 3 d, 7 d, 10 d and 14 d post administration of ZrO_2-NPs, with apparent decreases in the SOD activity and/or significant increases in the MDA level compared to the control.

Persistent and serious oxidative stress likely contributes to the inflammatory process through the activation of inflammation-related genes and transcription factors. The inflammatory cytokine expressions in the liver were therefore evaluated. The inflammatory response results (Fig. 2D) indicate that ZrO_2-NP exposure caused a continuous release of inflammatory cytokines (IL-1α, IL-1β, IL-6, IL-12, and TNF-α) in the liver. The induction of oxidative stress after translocation to the targeted organs could activate immune cells to release inflammatory cytokines such as TNF-α and IL-1β, which would further

stimulate the expression of IL-6 and IL-8 [29]. It was revealed that NPs-induced ROS and TNF-α were important activators in inducing DNA strand breaks [30]. Thus, the tissue damage induced by ZrO_2-NPs might be attributed to continuous inflammatory cytokine expressions and oxidative stresses.

Liver Function Analysis. To further estimate the liver function damage, the serum biochemical parameters were assayed. Fig. 2E demonstrates the changes of biochemical parameters in the liver after the administration of ZrO_2-NPs at six time points. The activities of ALT and AST (P<0.01) in the liver 3 d, 7 d and 10 d after exposure to ZrO_2-NPs were significantly higher than those of the controls. The significant increase of the LDH content (P<0.05) in the liver 7 d and 10 d post injection with ZrO_2-NPs were detected. The activities of ALT, AST and LDH in ZrO_2-NPs-exposed liver samples increased significantly compared to the controls, indicating that ZrO_2-NPs could induce hepatic function damage (Fig. 2E).

Histopathological, Immunofluorescence Evaluation and Ultrastructure Observation. Histopathological evaluation proved the existence of steatosis and cell death in the liver. Excessive lipid droplet (LD) accumulation in hepatocytes can cause a lipotoxic response involving lysosome-dependent cell death [31]. Hepatic cord disorganizations were observed in the livers of rats 3 d and 7 d post exposure to ZrO_2-NPs (Fig. 3 C-F). Fatty degeneration of the liver cells was observed in the livers of rats 7 d post exposure to ZrO_2-NPs (Fig. 3 E, F). Liver samples taken 10 d post exposure to ZrO_2-NPs showed more severe hepatic cord disorganizations than did those taken 3 d post injection (Fig. 3 G, H). Significantly larger numbers of Ki-67 positively stained cells were observed in the liver 3d and 7d post injection (Fig. 3). The Ki-67 immunochemical test results (Fig. 4) reveal the ZrO_2-NPs promotion effect on cell proliferative, indicating the increased possibility of an inflammatory response or tumor cell growth. Fig. 5 shows that the numbers of cells with nuclei positively stained by Tunel were significantly higher among the live cells 7 d after ZrO_2-NPs exposure (P<0.01) than among the control cells, which indicates increased cellular apoptosis 7 d after ZrO_2-NP exposure. Non-alcoholic fatty liver disease (NAFLD) is a chronic liver disease that refers to a wide spectrum of liver diseases that develop progressively from simple steatosis to non-alcoholic steatohepatitis (NASH), fibrosis, and even cirrhosis [32, 33]. It is generally acknowledged that oxidative stress, inflammation, steatosis and cell death play essential roles in the development of NAFLD, although the pathogenesis of NAFLD has not been fully discovered [34]. Thus, based on the histopathological and immunofluorescence observation results, as well as the oxidative stress and inflammatory response tests, ZrO_2-NPs exposure is likely to cause NAFLD. The ultrastructural changes in the liver show the generation of autophagosomes, as presented in Fig. 6. Reportedly, autophagy activation could alleviate hepatosteatosis [35].

RNA-Seq and RT-qPCR Analysis. According to the studies above, ZrO_2-NPs induced hepatic stress, especially by 7 d post exposure. Therefore, microarray analysis of the genes expressed in the liver 7 d post injection was conducted. In total, 68 gene expressions in the ZrO_2-NPs-treatment groups (32 upreglated and 36 downregulated) were significantly different from those of the control group. All DEGs identified in the liver samples after exposure to ZrO_2-NPs were annotated for GO enrichment analysis. Following exposure to ZrO_2-NPs, the DEGs were assigned to 44 GO terms in all three ontologies

(biological processes, cellular components and molecular functions), and biological processes appeared to capture most of these terms (Fig. 7A).

To identify the related pathways that induce liver tissue damage after exposure to ZrO_2-NPs, we characterized the pathways in which the DEGs were involved in the KEGG database. The top first-level KEGG pathways were identified as related to metabolism, followed by organismal systems and human diseases (Fig. 7B). Top third-level KEGG pathway terms are shown in Tab. 2. Heat maps were generated to show the expression values of differently expressed transcripts for each group by color based on the read count, with the color changing from red to blue (Fig. 7C). The gene expression changes (>2 fold) in the rat livers 7 d post injection with ZrO_2-NPs (P>0.80) are shown in Tab. 3.

To further explore the mechanism of ZrO_2-NPs-induced toxicity in the liver, selected DEGs were validated by RT-qPCR. The RT-qPCR analysis results (Fig. 7D) showed that ZrO_2-NP exposure caused the upregulation of P53, Foxo1, Gadd45g, P21, Caspase3, and PPARα and the downregulation of Igfbp2 and Akt in the liver in response to the ZrO_2-NP treatment. The most differentially expressed gene in the liver was Bcl6, which showed the highest fold change of 5.11.

In Vitro Study

Cytotoxicity and ROS production from ZrO_2-NPs Exposure. Treatment with ZrO_2-NPs could induce significant cell death (>50 %) at a dose of 750 μg/ml after 24 h coincubation (Fig. 8A). Treatment with ZrO_2-NPs could induce significant cell death (>50 %) at a dose of 1000 μg/ml after 12 h coincubation, and it caused the same toxic effect at 500 ug/mL after 24 h exposure (Fig. 8A). Our results showed that ZrO_2-NPs triggered cytotoxicity in a dose- and time- dependent manner. Our findings were consistent with those of previous studies reported recently [7, 8, 36] .

To further examine the effect of ZrO_2-NPs on the cell membrane permeability, an LDH assay was conducted in Hepg2 cells incubated with a series of concentrations of ZrO_2-NPs for 12 h and 24 h. The percentage of LDH released into the culture medium was measured as an index of cellular death, and the results are presented in Figure 8B. The toxic effect was consistent with that observed in the cell viability evaluation results, also demonstrating a dose- and time- dependent manner. Fig. 8C demonstrates that the ROS levels of the cells exposed to ZrO_2-NPs at concentrations from 0 ug/mL to 1000 μg/ml after 6 h exposure, which increased with the elevation of the ZrO_2-NPs concentration.

ZrO_2-NPs induced lipid accumulation and apoptosis. Excessive lipid droplet (LD) accumulation in hepatocytes can drive a lipotoxic response. As shown by the in vivo study, hepatosteatosis, extra ROS generation, inflammatory responses and lipid metabolism gene changes were observed. We assume that hepatosteatosis could be the main mechanism behind ZrO_2-NPs-induced liver toxicity. To further explore this assumption, an in vitro study for the evaluation of lipid accumulations and lipid metabolism-related protein expression changes was therefore carried out. According to the TG and TC accumulation evaluations (Fig. 9A), Hepg2 cell showed increased lipid accumulations upon exposure to ZrO_2-NPs

starting from a concertation of 500 μg/mL. Fig. 9 B, C and D show the upregulation of Foxo1 and the downregulation of Igfbp2 and Akt. The overexpression of Igfbp2 has been shown to reverse diabetes and steatosis in obese mice [37]. Downregulation of Igfbp2 was reported to be the maker of NAFLD [38]. As a symptom of metabolic disorders, hepatic lipid accumulation is strongly associated with insulin resistance [39]. Insulin resistance, which is characteristic of IRs/Akt depression, has been recognized for many years to be an essential component of NAFLD pathogenesis [40]. The downregulation of Akt reduces the phosphorylation of Foxo1, which leads to Foxo1 activation and results in the promotion of NAFLD [41]. Thus, based on our study, ZrO_2-NPs are likely to induce hepatosteatosis via activation of the Akt/Foxo1 pathway or downregulation of Igfbp2.

A recent study investigated the toxicol profiles of several metal oxide NPs (including some rare earth oxides and transition metal oxides) in hepatocytes and proved that they could induce hepatocyte death by apoptosis [36]. However, the exact mechanism of ZrO_2-NPs-induced hepatocyte death is unknown. As shown by Cell viability evaluation (Fig. 8A), ZrO_2-NPs require a relatively higher concentration (>250 μg/mL) to cause a reduced percentage of viability. Fig. 10 shows that ZrO_2-NPs exposure (250 μg/mL) could induce apoptosis in Hepg2 cells at 24 h, which is consistent with the in vivo Tunel test results. Expressions of proapoptotic proteins—including P53, Bax, Caspase3, Gadd45g, and Bcl6 increased in the Hepg2 cells (Fig. 10C). Meanwhile, the expression of antiapoptotic protein Bcl2 decreased in the Hepg2 cells (Fig. 10C). Additionally, cell-cycle analysis (Fig. 10B) demonstrated that Hepg2 cell exposure to 250 μg/mL ZrO_2-NPs resulted in G1/G0 arrest of the Hepg2 cells, allowing cellular repair or resulting in the activation of apoptosis signaling when severe DNA damage occurred [42]. The overexpression of cell cycle-regulating proteins (P21 and Gadd45g) was also detected (Fig. 10C). These results have shown that exposure of HepG2 cells to ZrO_2-NPs may trigger cell apoptosis through the upregulation of P53 and subsequently activate Bcl6 expression, thereby increasing the Bax/Bcl2 ratio and finally activating Caspase3 expression.

Conclusion

We investigated the hepatic biodistribution and toxicological effects of ZrO_2-NPs after intravenous administration in vivo and the toxicological mechanism toward hepatocytes in vitro. The liver showed continuous ZrO_2-NPs accumulation over a 28-d period. Moreover, ZrO_2-NPs induced oxidative stress and increased inflammatory responses and functional injury in the liver. Hepasteatosis and cell death were observed in histopathological and immunohistochemical studies. RNA-seq showed that the main pathways identified were involved in metabolism, cellular process, and human diseases. Meanwhile, the results of the in vitro studies demonstrated that ZrO_2-NPs exposure resulted in cytotoxicity in Hepg2 cells in a dose- and time-dependent manner. Then ZrO_2-NPs were proven to induce oxidative stress, lipid accumulation, cell apoptosis, Igfbp2 downregulation, Akt-mediated signaling pathway activation and P53-mediated signaling pathway activation.

Overall, the present study indicates the potential toxicity of ZrO_2- NPs toward the liver and a possible risk for NAFLD after exposure to a certain dosage and/or over a certain time period. There is potential concern over ZrO_2-NPs hepatoxicity in biomedical applications and occupational exposure through large-scale production. However, the present study is a primarily study involving the ZrO_2-NPs-triggered hepatic toxicological mechanism. Further studies involving precious gene expression analysis at both the mRNA and protein levels with the inhibition or promotion of key genes are needed to verify the ZrO_2-NPs-induced hepatic toxicological pathways.

Abbreviations

ZrO_2- NPs: ZrO_2-nano particles; RNA-Seq: RNA-sequencing; TEM: transmission electron microscope; ALT: alanine aminotransferase; AST: aspartate aminotransferase; LDH: lactate dehydrogenase; NAFLD: non-alcoholic fatty liver disease; DEGs: differentially expressed genes.

Declarations

Acknowledgements

Not applicable.

Authors' contributions

Ting Sun designed the study, performed the experiments, interpreted the data, prepared the figures and wrote the manuscript. Lingling Ou, Xiaozhen Zhan, Xiaoli Feng, Jia Liu, Wenxin Zhao, Rui Huang, Suhan Yin, Xiangning Liu performed the experiments. Longquan Shao, Ting Sun and Renfa Lai provided laboratory space and funding and directed the project. All authors have read, corrected and approved the manuscript.

Funding

This work was supported by the Natural Science Foundation of Guangdong Province (2019A1515010263), the Science and Technology Planning Project of Guangzhou (201904010059), the China Postdoctoral Science Foundation (2017M622742), and the Guangdong Medical Science and Technology Research Fund Project (A2018081).

Availability of data and materials

The datasets used and/or analyzed in the current study are available from the corresponding author on reasonable request.

Ethics approval and consent to participate

Not applicable.

Consent for publication

Not applicable.

Competing interests

The authors declare that they have no competing interests.

Author details

[a] Medical center of Stomatology, The First Affiliated Hospital, Jinan University, Guangzhou, 510630, China

[b] Department of Stomatology, Nanfang Hospital, Southern Medical University, Guangzhou 510515, China

[c] Stomatological Hospital, Southern Medical University, Guangzhou 510280, China

References

1. Wagner A, Belli R, Stotzel C, Hilpert A, Muller FA, Lohbauer U. Biomimetically- and hydrothermally-grown HAp nanoparticles as reinforcing fillers for dental adhesives. J Adhes Dent. 2013;15(5):413-22.
2. Thoma DS, Benic GI, Munoz F, Kohal R, Sanz Martin I, Cantalapiedra AG, et al. Histological analysis of loaded zirconia and titanium dental implants: an experimental study in the dog mandible. J Clin Periodontol. 2015;42(10):967-75.
3. Wang R, Bao S, Liu F, Jiang X, Zhang Q, Sun B, et al. Wear behavior of light-cured resin composites with bimodal silica nanostructures as fillers. Mater Sci Eng C Mater Biol Appl. 2013;33(8):4759-66.
4. Kumar S, Kumar S, Tiwari S, Srivastava S, Srivastava M, Yadav BK, et al. Biofunctionalized Nanostructured Zirconia for Biomedical Application: A Smart Approach for Oral Cancer Detection. Adv Sci (Weinh). 2015;2(8):1500048.
5. Bencsik A, Lestaevel P, Guseva Canu I. Nano- and neurotoxicology: An emerging discipline. Prog Neurobiol. 2018;160:45-63.
6. Park EJ, Lee GH, Han BS, Lee BS, Lee S, Cho MH, et al. Toxic response of graphene nanoplatelets in vivo and in vitro. Archives of toxicology. 2015;89(9):1557-68.
7. Alzahrani FM, Katubi KMS, Ali D, Alarifi S. Apoptotic and DNA-damaging effects of yttria-stabilized zirconia nanoparticles on human skin epithelial cells. Int J Nanomedicine. 2019;14:7003-16.
8. Ye M, Shi B. Zirconia Nanoparticles-Induced Toxic Effects in Osteoblast-Like 3T3-E1 Cells. Nanoscale Res Lett. 2018;13(1):353.
9. Yang Y, Bao H, Chai Q, Wang Z, Sun Z, Fu C, et al. Toxicity, biodistribution and oxidative damage caused by zirconia nanoparticles after intravenous injection. Int J Nanomedicine. 2019;14:5175-86.

10. Sun T, Liu G, Ou L, Feng X, Chen A, Lai R, et al. Toxicity Induced by Zirconia Oxide Nanoparticles on Various Organs After Intravenous Administration in Rats. Journal of biomedical nanotechnology. 2019;15(4):728-41.
11. Hoekstra LT, de Graaf W, Nibourg GA, Heger M, Bennink RJ, Stieger B, et al. Physiological and biochemical basis of clinical liver function tests: a review. Annals of surgery. 2013;257(1):27-36.
12. Lin Q, Deng D, Song X, Dai B, Yang X, Luo Q, et al. Self-Assembled "Off/On" Nanopomegranate for In Vivo Photoacoustic and Fluorescence Imaging: Strategic Arrangement of Kupffer Cells in Mouse Hepatic Lobules. ACS Nano. 2019;13(2):1526-37.
13. Zhang YN, Poon W, Tavares AJ, McGilvray ID, Chan WCW. Nanoparticle-liver interactions: Cellular uptake and hepatobiliary elimination. J Control Release. 2016;240:332-48.
14. Yu M, Zheng J. Clearance Pathways and Tumor Targeting of Imaging Nanoparticles. ACS Nano. 2015;9(7):6655-74.
15. Liu T, Li L, Teng X, Huang X, Liu H, Chen D, et al. Single and repeated dose toxicity of mesoporous hollow silica nanoparticles in intravenously exposed mice. Biomaterials. 2011;32(6):1657-68.
16. Moghimi SM, Hunter AC, Murray JC. Long-circulating and target-specific nanoparticles: theory to practice. Pharmacological reviews. 2001;53(2):283-318.
17. Yi-Nan, Zhang, Wilson, Poon, Anthony, J., et al. Nanoparticle–liver interactions: Cellular uptake and hepatobiliary elimination.
18. Tarazona S, Garcia-Alcalde F, Dopazo J, Ferrer A, Conesa A. Differential expression in RNA-seq: a matter of depth. Genome Res. 2011;21(12):2213-23.
19. Liu T, Li L, Fu C, Liu H, Chen D, Tang F. Pathological mechanisms of liver injury caused by continuous intraperitoneal injection of silica nanoparticles. Biomaterials. 2012;33(7):2399-407.
20. Balasubramanian SK, Jittiwat J, Manikandan J, Ong CN, Yu LE, Ong WY. Biodistribution of gold nanoparticles and gene expression changes in the liver and spleen after intravenous administration in rats. Biomaterials. 2010;31(8):2034-42.
21. The One Year Fate of Iron Oxide Coated Gold Nanoparticles in Mice %J Acs Nano.9(8):150721103810005.
22. Wohlleben W, Driessen MD, Raesch S, Schaefer UF, Schulze C, Vacano B, et al. Influence of agglomeration and specific lung lining lipid/protein interaction on short-term inhalation toxicity. Nanotoxicology. 2016;10(7):970-80.
23. Chen YS, Hung YC, Lin LW, Liau I, Hong MY, Huang GS. Size-dependent impairment of cognition in mice caused by the injection of gold nanoparticles. Nanotechnology. 2010;21(48):485102.
24. Sun T, Zhang YS, Pang B, Hyun DC, Yang M, Xia Y. Engineered nanoparticles for drug delivery in cancer therapy. Angewandte Chemie (International ed in English). 2014;53(46):12320-64.
25. He C, Hu Y, Yin L, Tang C, Yin C. Effects of particle size and surface charge on cellular uptake and biodistribution of polymeric nanoparticles. Biomaterials. 2010;31(13):3657-66.

26. Liu Y, Wang Z, Liu Y, Zhu G, Jacobson O, Fu X, et al. Suppressing Nanoparticle-Mononuclear Phagocyte System Interactions of Two-Dimensional Gold Nanorings for Improved Tumor Accumulation and Photothermal Ablation of Tumors. ACS Nano. 2017;11(10):10539-48.
27. Wang H, Thorling CA, Liang X, Bridle KR, Grice JE, Zhu Y, et al. Diagnostic imaging and therapeutic application of nanoparticles targeting the liver.3(6):939-58.
28. Longmire M, Choyke PL, Kobayashi H. Clearance properties of nano-sized particles and molecules as imaging agents: considerations and caveats. Nanomedicine (Lond). 2008;3(5):703-17.
29. Chan EWL, Krishnansamy S, Wong C, Gan SY. The NLRP3 inflammasome is involved in the neuroprotective mechanism of neural stem cells against microglia-mediated toxicity in SH-SY5Y cells via the attenuation of tau hyperphosphorylation and amyloidogenesis. Neurotoxicology. 2019;70:91-8.
30. El-Boghdady NA, Abdeltawab NF, Nooh MM. Resveratrol and Montelukast Alleviate Paraquat-Induced Hepatic Injury in Mice: Modulation of Oxidative Stress, Inflammation, and Apoptosis. Oxidative medicine and cellular longevity. 2017;2017:9396425.
31. Galluzzi L, Vitale I, Aaronson SA, Abrams JM, Adam D, Agostinis P, et al. Molecular mechanisms of cell death: recommendations of the Nomenclature Committee on Cell Death 2018. Cell death and differentiation. 2018;25(3):486-541.
32. Sanyal AJJHR. NASH: A global health problem.41(7):670-4.
33. Ban LA, Shackel NA, McLennan SV. Extracellular Vesicles: A New Frontier in Biomarker Discovery for Non-Alcoholic Fatty Liver Disease. International journal of molecular sciences. 2016;17(3):376.
34. Wesolowski SR, Kasmi KC, Jonscher KR, Friedman JE. Developmental origins of NAFLD: a womb with a clue. Nat Rev Gastroenterol Hepatol. 2017;14(2):81-96.
35. Sinha RA, Farah BL, Singh BK, Siddique MM, Li Y, Wu Y, et al. Caffeine stimulates hepatic lipid metabolism by the autophagy-lysosomal pathway in mice. Hepatology (Baltimore, Md). 2014;59(4):1366-80.
36. Mirshafiee V, Sun B, Chang CH, Liao YP, Jiang W, Jiang J, et al. Toxicological Profiling of Metal Oxide Nanoparticles in Liver Context Reveals Pyroptosis in Kupffer Cells and Macrophages versus Apoptosis in Hepatocytes. ACS Nano. 2018;12(4):3836-52.
37. Ahrens M, Ammerpohl O, von Schonfels W, Kolarova J, Bens S, Itzel T, et al. DNA methylation analysis in nonalcoholic fatty liver disease suggests distinct disease-specific and remodeling signatures after bariatric surgery. Cell metabolism. 2013;18(2):296-302.
38. Dali-Youcef N, Vix M, Costantino F, El-Saghire H, Lhermitte B, Callari C, et al. Interleukin-32 Contributes to Human Nonalcoholic Fatty Liver Disease and Insulin Resistance. Hepatology communications. 2019;3(9):1205-20.
39. Jian T, Ding X, Wu Y, Ren B, Li W, Lv H, et al. Hepatoprotective Effect of Loquat Leaf Flavonoids in PM2.5-Induced Non-Alcoholic Fatty Liver Disease via Regulation of IRs-1/Akt and CYP2E1/JNK Pathways. International journal of molecular sciences. 2018;19(10).

40. Choudhury J, Sanyal AJJCiLD. Insulin resistance and the pathogenesis of nonalcoholic fatty liver disease. 2004;8(3):575-94, ix.
41. Liu XL, Pan Q, Cao HX, Xin FZ, Zhao ZH, Yang RX, et al. Lipotoxic Hepatocyte-Derived Exosomal miR-192-5p Activates Macrophages via Rictor/Akt/FoxO1 Signaling in NAFLD. Hepatology (Baltimore, Md). 2019.
42. Wu J, Wang C, Sun J, Xue Y. Neurotoxicity of silica nanoparticles: brain localization and dopaminergic neurons damage pathways. ACS Nano. 2011;5(6):4476-89.

Tables

Tab. 1 Primer sequences used in the RT-qPCR analysis.

Gene	Forward primer	Reverse primer
P53	CTACTAAGGTCGTGAGACGCTGCC	TCAGCATACAGGTTTCCTTCCACC
Foxo1	ATGCTCAATCCAGAGGGAGG	ACTCGCAGGCCACTTAGAAAA
Bcl6	AAAGGCCGGACACCAGTTTT	CATGGCGGGTGAACTGGATA
Gadd45g	GTCCTGAATGTGGACCCTGAC	GATGCAATGCAAGTCTCCCG
Igfbp2	GACGTTACGCTGTTACCCCA	GGTCATCCTCACTGTCTGCAA
P21	TTGTGATATGTACCAGCCACAGG	GCGAAGTCAAAGTTCCACCG
Akt	ATGAGCGACGTGGCTATTGT	TGAAGGTGCCATCATTCTTG
Caspase3	TGGCATTGAGACAGACA	GGCACAAAGCGACTG
PPARα	GGGACAGACTGACACCTTACTT	ATGGGACCCTTATCAATCCTA
Gadph	AAGGTGAAGGTCGGAGTCAA	AATGAAGGGGTCATTGATGG

Tab. 2 Top third-level KEGG pathway terms in rat livers 7 d post injection with ZrO_2-NPs.

	Third pathway terms	Pathway ID	DEGs genes with pathway annotation	All genes with pathway annotation	First pathway terms	*P* Values	Second pathway terms
1	Retinol metabolism	Ko00830	9	82	Metabolism	4.18^{-11}	Metabolism of cofactors and vitamins
2	*Metabolic pathways*	Ko01100	23	1436	Metabolism	3.93^{-9}	Global and overview maps
3	Linoleic acid metabolism	Ko00591	6	41	Metabolism	1.50^{-8}	Lipid metabolism
4	*Steroid hormone biosynthesis*	Ko00140	7	90	Metabolism	7.93^{-8}	Lipid metabolism
5	Chemical carcinogenesis	Ko05204	7	96	Human Diseases	1.24^{-7}	Cancers: overview
8	PPAR signaling pathway	Ko03320	6	101	Organismal Systems	3.50^{-6}	Endocrine system
9	Arachidonic acid metabolism	Ko00590	5	105	Metabolism	6.98^{-5}	Lipid metabolism
10	Bile secretion	Ko04976	4	110	Organismal Systems	0.00	Digestive system
11	Fatty acid metabolism	Ko01212	3	55	Metabolism	0.00	Global and overview maps
12	Carbon metabolism	Ko01200	4	133	Metabolism	0.00	Global and overview maps
13	Steroid biosynthesis	Ko00100	2	26	Metabolism	0.01	Lipid metabolism
14	P53 signaling pathway	Ko04068	3	85	Cellular Processes	0.01	Cell growth and death
15	Alpha-linolenic acid metabolism	ko00592	2	28	Metabolism	0.01	Lipid metabolism

Tab. 3 Gene expression changes (>2 fold) in rat livers 7 d post injection with ZrO_2-NPs.

Gene symble	Gene	Fold change	*P* value
Hemoglobin alpha, adult chain 1	Hba-a1	4.76	0.83
Patatin-like phospholipase domain-containing 3	Pnpla3	4.31	0.97
Megalencephalic leukoencephalopathy with subcortical cysts 1	Mlc1	2.984	0.86
MicroRNA 762	Mir762	2.88	0.90
Patatin-like phospholipase domain-containing 5	Pnpla5	2.53	0.87
B-cell CLL/lymphoma 6	Bcl6	2.26	0.873
Lipin 1	Lpin1	2.1	0.90
Ribosomal protein L37a	Rpl37a	2.13	0.83
MicroRNA 6318	Mir6318	2.06	0.85
Glucokinase	Gck	2.03	0.91
Hemoglobin, alpha 1	Hba1	-2.01	0.93
Isopentenyl-diphosphate delta isomerase 1	Idi1	-2.05	0.89
Hemoglobin subunit beta	Hbb	-2.10	0.93
Similar to C030030A07Rik protein	LOC500354	-2.13	0.81
Hemoglobin, beta adult major chain	Hbb-b1	-2.23	0.91
Beta-globin	LOC689064	-2.26	0.91
Indolethylamine N-methyltransferase	Inmt	-2.72	0.94
Insulin-like growth factor binding protein 2	Igfbp2	-2.97	0.94
Membrane bound O-acyltransferase domain containing 7	Mboat7l1	-8.22	0.83

According to the gene expression analysis software, differences were statistically significant when $P>0.80$.

Figures

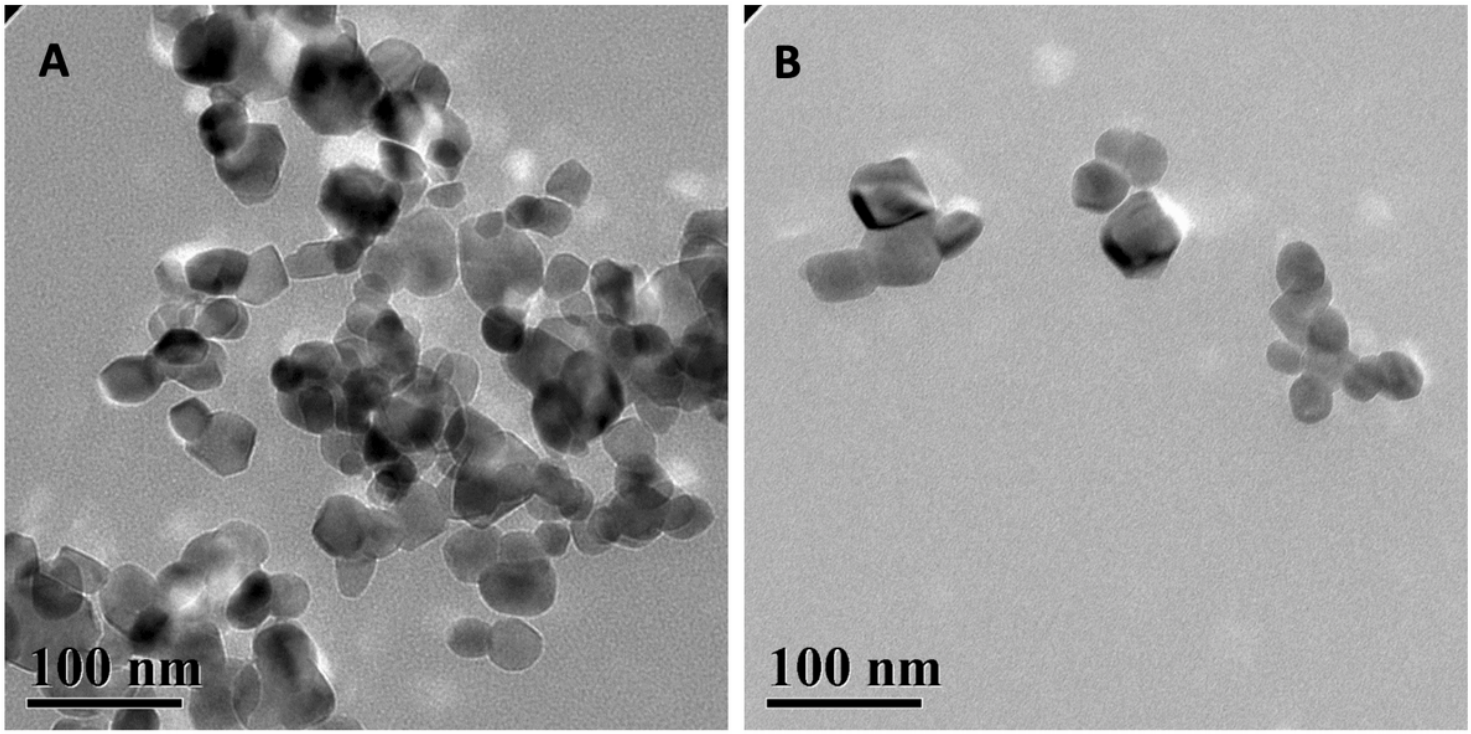

Figure 2

Characterization of the primary ZrO2-NPs. (A, B) TEM image of the ZrO2-NPs.

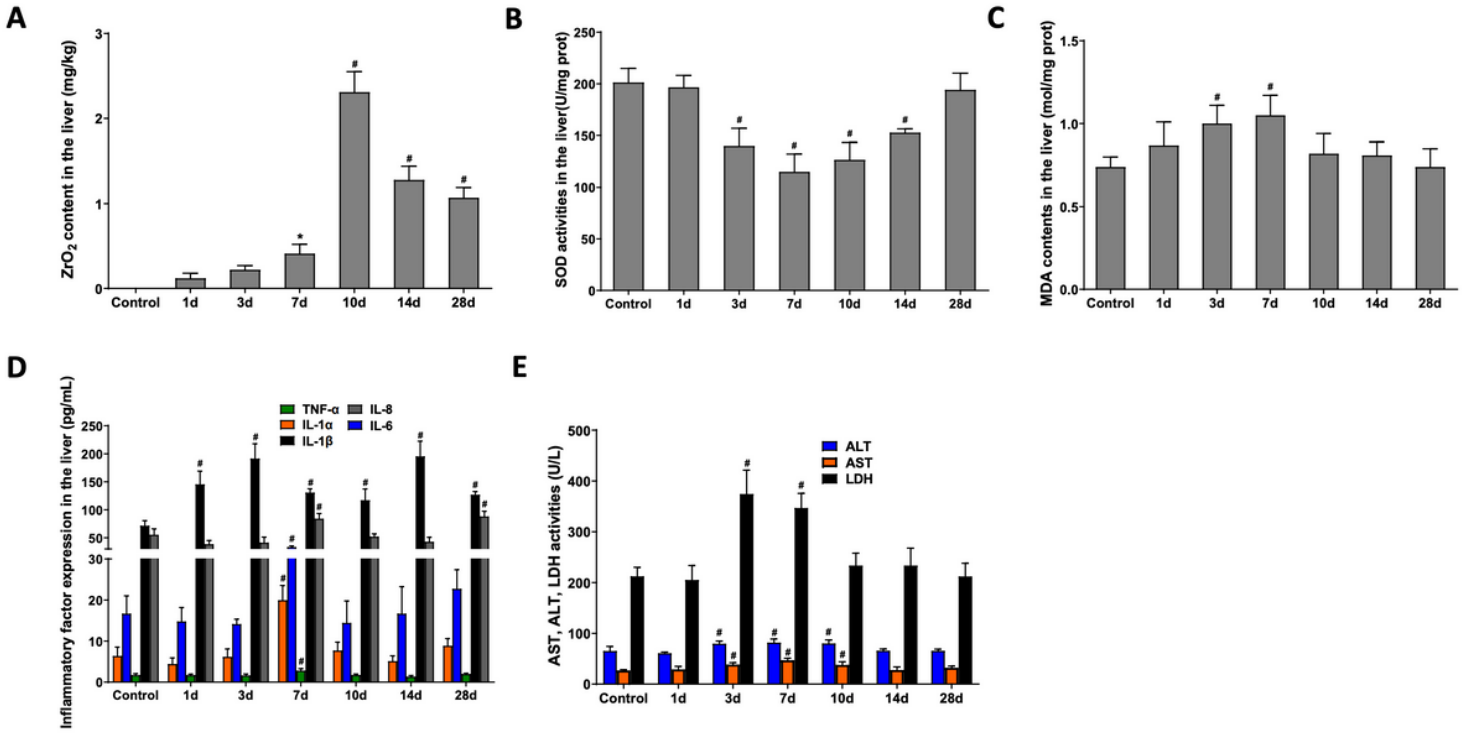

Figure 4

Biodistribution of ZrO2-NPs and ZrO2-NPs-induced changes in the liver. A Biodistributions of ZrO2-NPs in the liver after 1 d, 3 d, 7 d, 10 d, 14 d and 28 d exposure. B Activities of SOD in the liver at six time points after exposure to ZrO2-NPs. C Levels of MDA in the liver at six time points after exposure to ZrO2-NPs. D Levels of TNF-α, IL-1α, IL-1β, IL-6 and IL-8 in the liver at six time points after exposure to ZrO2-NPs. E AST, ALT, and LDH activities in the liver. Data represent the mean ± SD (n=10). Significance versus control: #P< 0.01, *P< 0.05.

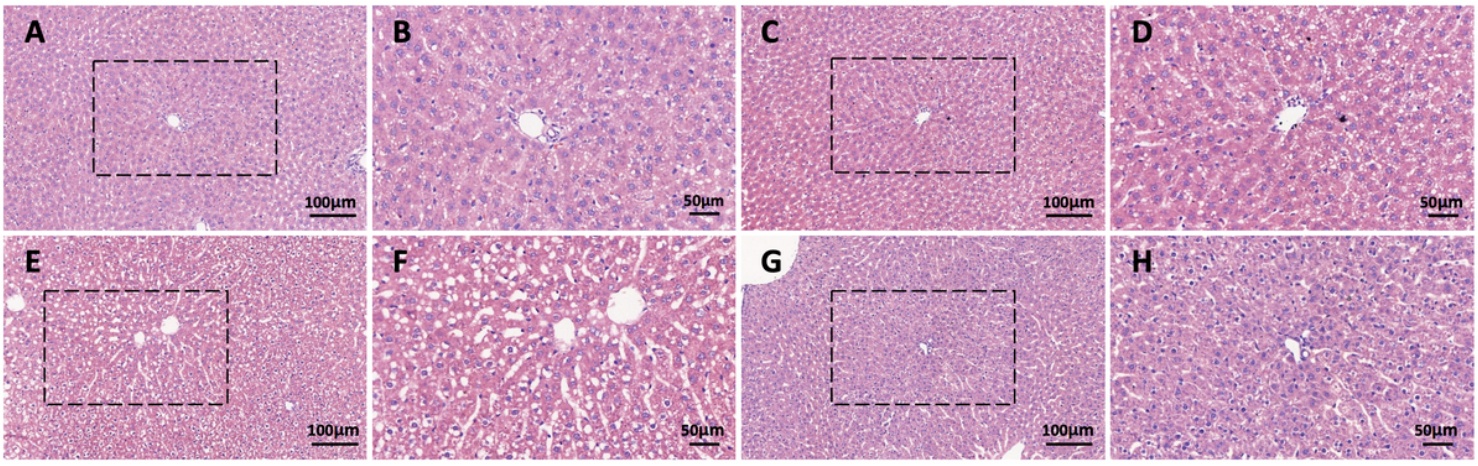

Figure 5

H&E-staining pathological analysis of the liver after ZrO2-NPs exposure. A and B Liver control sample. C and D Liver sample 3 d post injection. E and F Liver sample 7 d post injection. G and H Liver sample 10 d post injection.

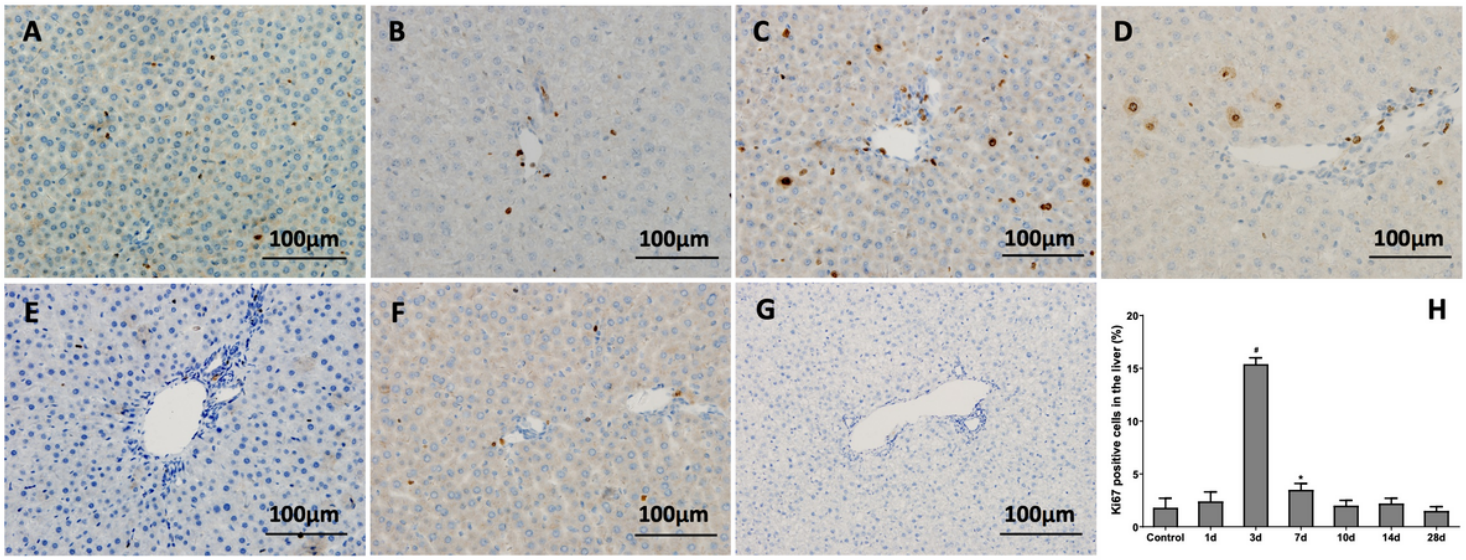

Figure 7

Ki-67 immunohistochemical analysis of the liver after ZrO2-NPs exposure. Liver control sample (A). Liver sample at 1 d (B), 3 d (C), 7 d (C), 10 d (D), 14 d (E), and 28 d (F) post injection. Statistic Ki-67 positive cells in in the liver (H).

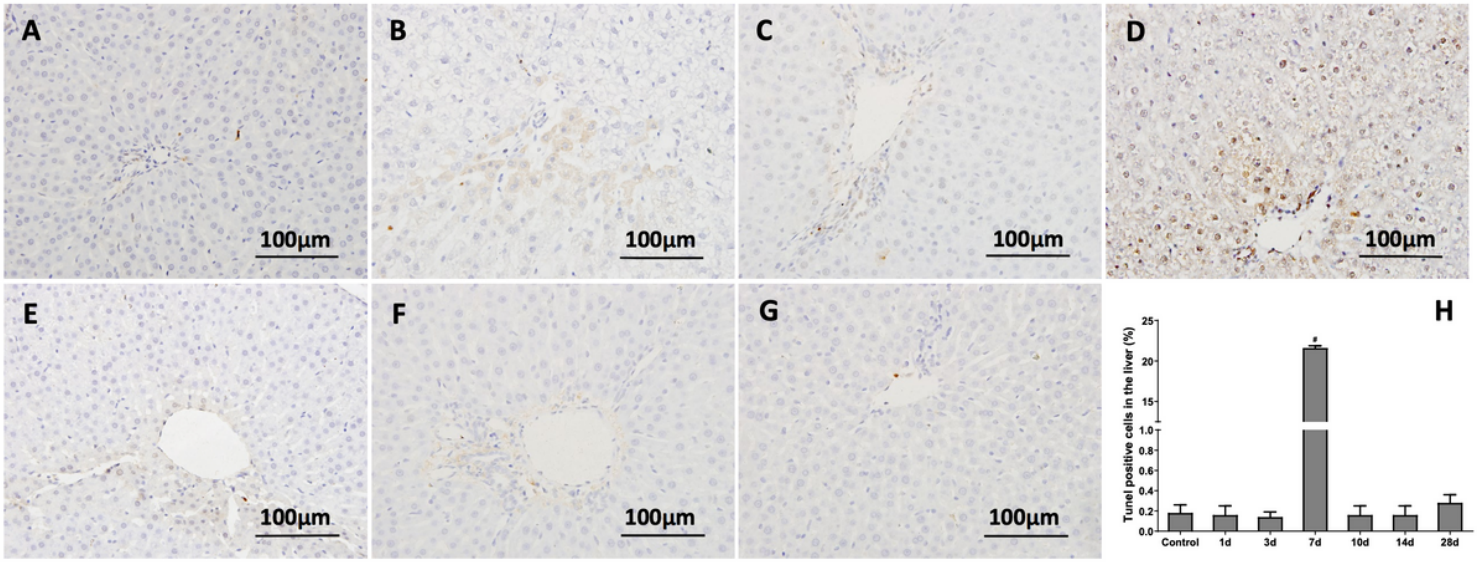

Figure 10

Tunel immunohistochemical analysis of the liver after ZrO2-NPs exposure. Liver control sample (A). Liver sample at 1 d (B), 3 d (C), 7 d (C), 10 d (D), 14 d (E), and 28 d (F) post injection. Statistically Tunel-positive cells in the liver (H).

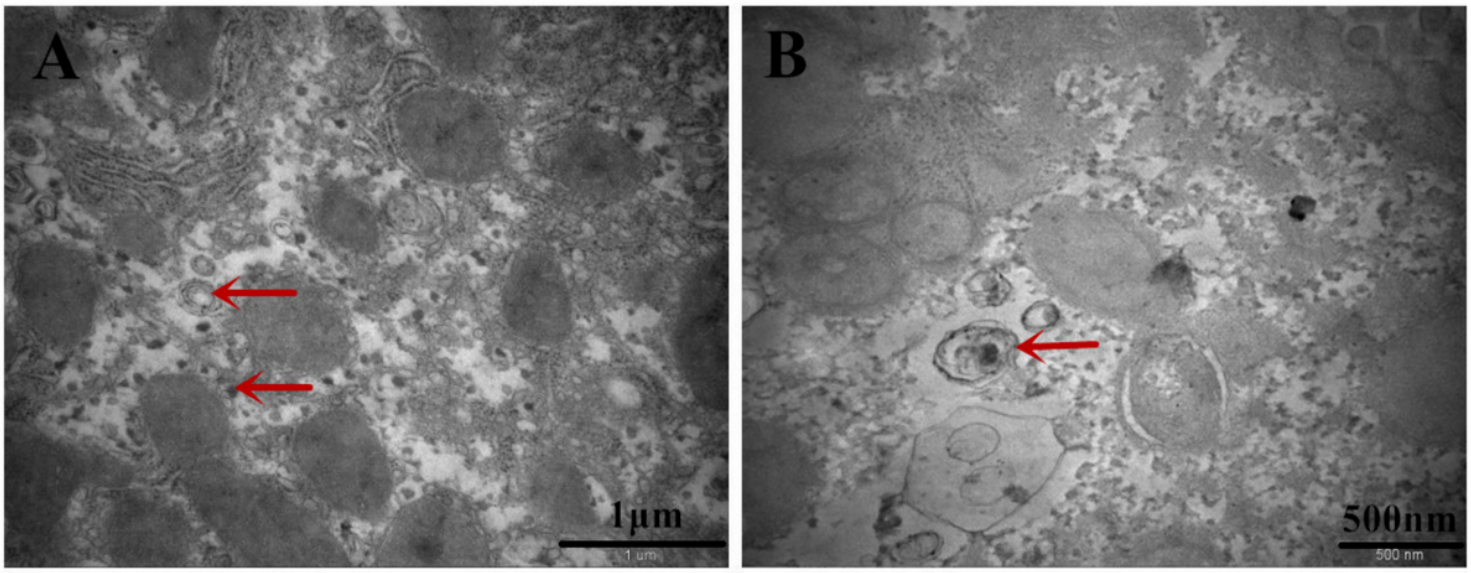

Figure 12

Ultrastructure of liver cells 7 d post exposure to the ZrO2-NPs. The red arrows indicate NPs in the liver cells and the induced autophagosomes.

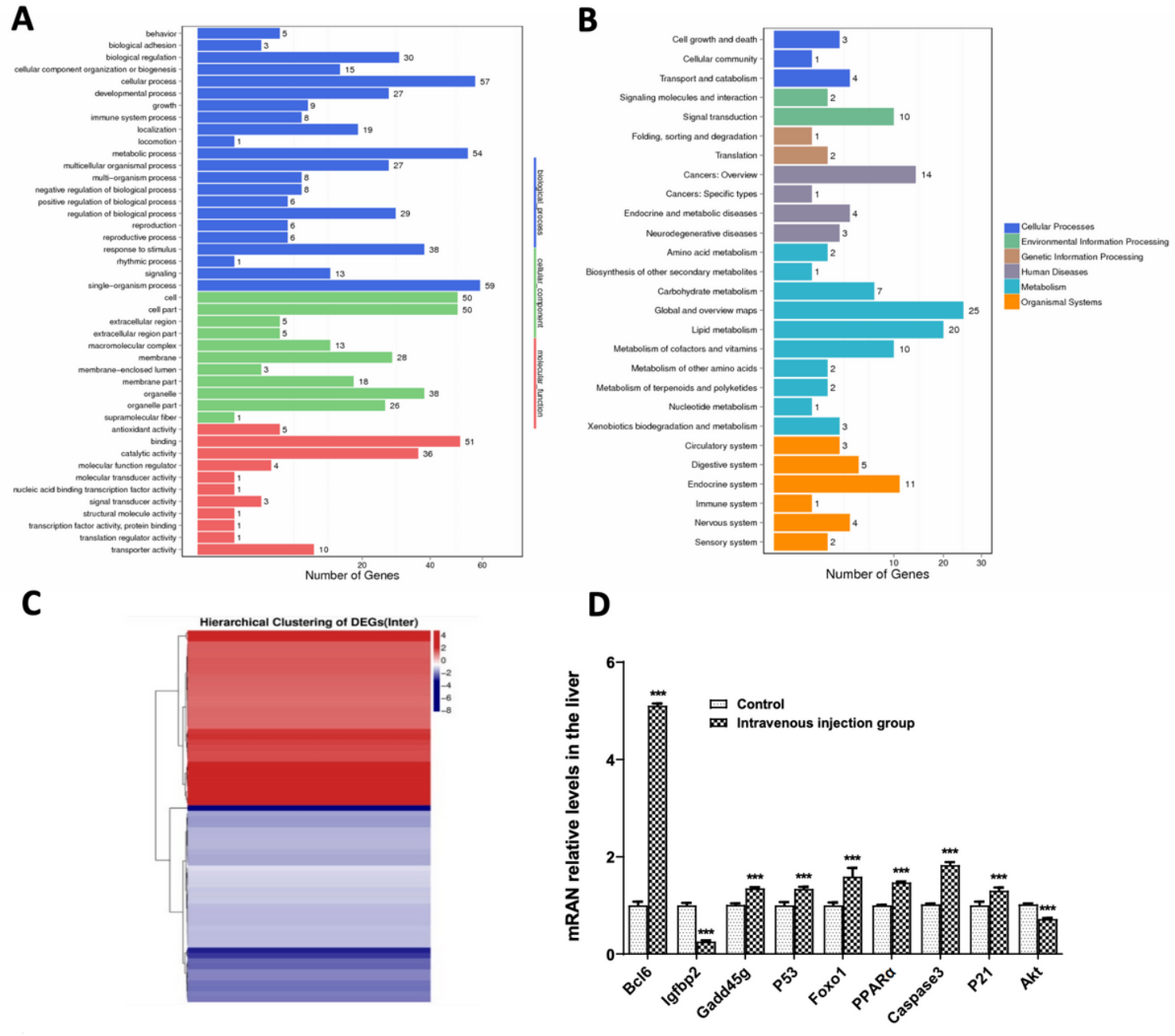

Figure 14

Gene expression analysis of the gene expression changes induced by ZrO2-NPs in the livers of 7 d post-injection rats. A GO terms determined by RNA-Seq analysis. B KEGG pathways determined by RNA-Seq analysis. C Heat map determined by RNA-Seq analysis. D qRT-PCR analysis of selected DEGs.

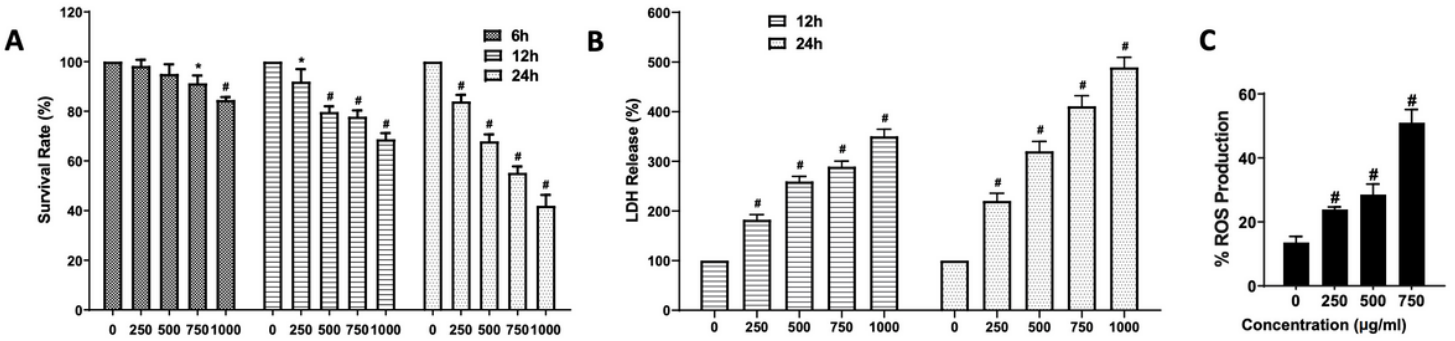

Figure 16

Effects of ZrO2-NPs on the cytotoxicity and oxidative stress of Hepg2 cells. A Viability of Hepg2 cells treated with ZrO2-NPs, as measured by the MTT assay. B LDH releases of Hepg2 cells treated with ZrO2-NPs. C ROS production (6 h incubation time) after treatment with ZrO2-NPs. n =5, #P< 0.01, *P< 0.05 compared to untreated cells in the same time-course line, respectively.

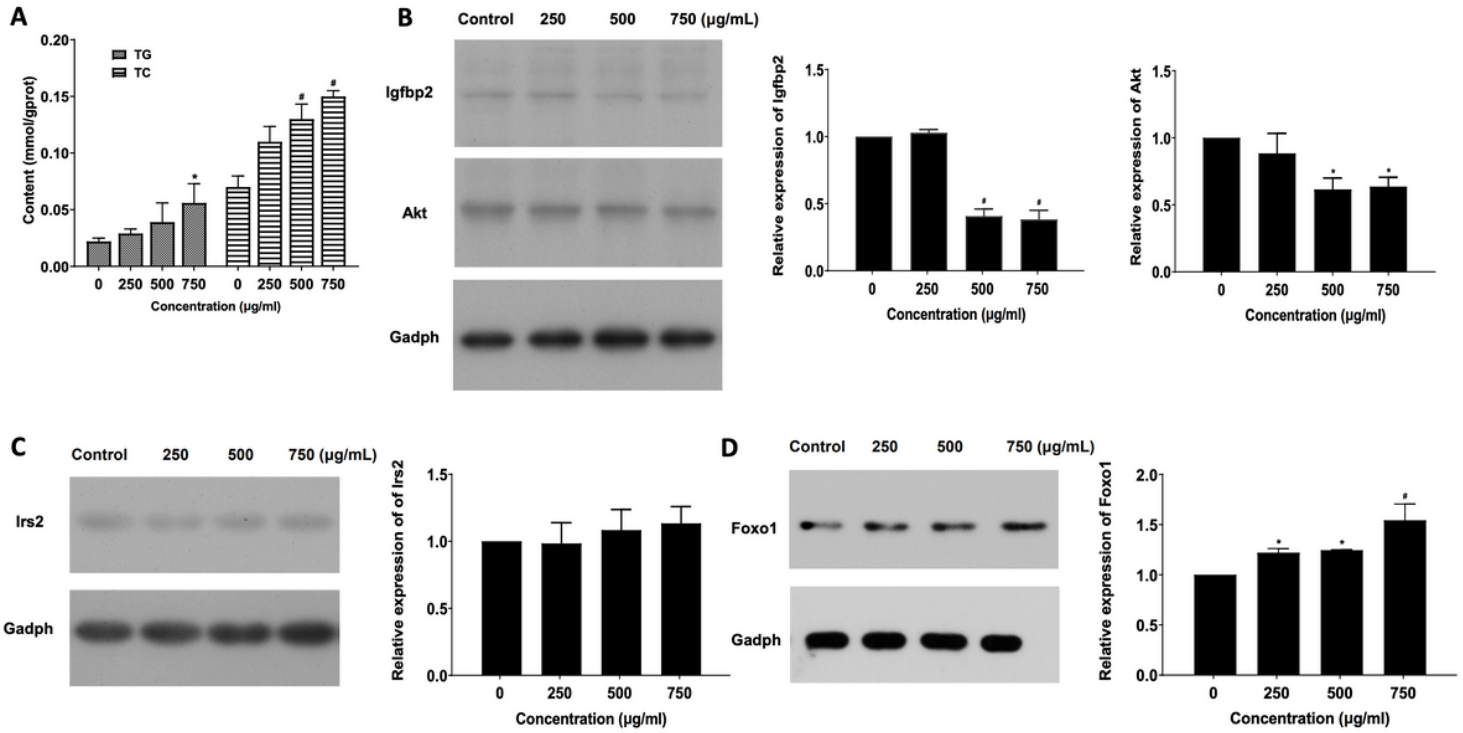

Figure 17

Analysis of the lipid accumulation of ZrO2-NPs-treated Hepg2 cells. A TG and TC contents of Hepg2 cells cultured with ZrO2-NPs. B, C, D Western blot analysis of Igfbp2, Akt, Irs2 and Foxo1 expressions in Hepg2 cells induced by ZrO2-NPs. n =3, #P< 0.01, *P< 0.05 when compared with the control.

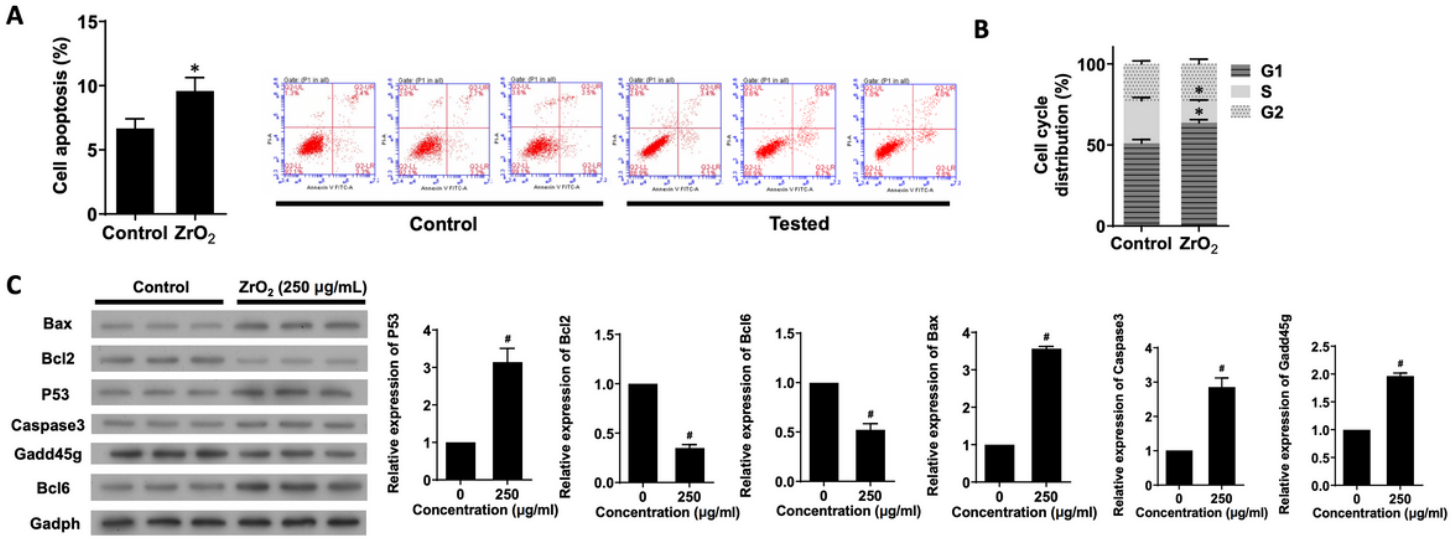

Figure 19

Analysis of the apoptosis and cell cycles of ZrO2-NPs-treated Hepg2 cells. A Apoptosis and cell death induced by ZrO2-NPs treatment in Hepg2 cells double-stained with PI- and FITC-labeled annexin V. B Cell cycle distribution of Hepg2 cells cultured with ZrO2-NPs. C Western blot analysis of P53, P21, Gadd45g, Bcl2, Bcl6, P53, Bax and Caspase3 expressions in Hepg2 cells induced by ZrO2-NPs. n =3, #P< 0.01, *P< 0.05 when compared with the control.